# Conservation Properties of the Hamiltonian Particle-Mesh method for the Quasi-Geostrophic Equations on a sphere

## MSc Thesis

Halldora Thorsdottir

1st of November, 2011

supervisor:

Prof. Dr. Jason Frank

UNIVERSITEIT VAN AMSTERDAM    CWI  Centrum Wiskunde & Informatica

**Abstract**

The Hamiltonian particle-mesh (HPM) method is used to solve the Quasi-Geostrophic model generalized to a sphere, using the Spherepack modeling package to solve the Helmholtz equation on a colatitude-longitude grid with spherical harmonics. The predicted energy conservation of a Poisson system is shown to be approximately retained and statistical mean-field theory is verified.

## Acknowledgements

# Contents

# Chapter 1

# Introduction

## 1.1 Solving chaotic dynamical systems

Attempts to predict the weather have long ago developed from being an art to being a science, despite the difficulties involved in forecasting chaotic behaviour. Using numerics to predict the weather was first tried and published by L.F.Richardson in 1922 [20]. Given the large error of his results, and likely also the time and effort which it required, it is not surprising that numerical predictions of weather were considered practically intractable until the invention of the computer in the mid-20th century. Shortly after that, the first successful numerical weather prediction saw light in the work of Charney, Fjørtoft and von Neumann in 1950 [6]. After that followed a period where ever more powerful computers were able to solve ever more complex models of higher resolution to a higher level of accuracy.

This rapid advancement is no longer the case, as the resolution of models has now reached the point where the separation between resolved and unresolved motions for certain atmospheric phenomena is less clear ([15], citations therein). This requires a greater understanding of the real atmosphere, as well as the numerical methods. For those purposes, simpler models have been popular study cases in order to gain insight into the underlying physical processes and to investigate the properties of numerical methods.

The detailed resolution needed for weather phenonema of public interest, such as rain, wind and fog, differs from the resolution required for climate simulation. Climate is typically characterized in terms of suitable averages over periods of a month or longer, taking into consideration the variability in time. As such, climate can be seen as the statistics of weather. Predicting the weather and climate far ahead in time translates in scientific language to solving chaotic dynamical systems on a long time interval. Such systems are known to be highly sensitive to initial conditions and thus long numerical simulations of them are very error-prone, meaning that any minute error

in measurements will eventually lead to large scale divergence [2]. Furthermore, in the case of numerical weather prediction, accurate initial conditions are rarely available. This makes simulating a single trajectory with any numerical accuracy a difficult goal.

The real goal of such simulations is therefore to obtain a data set suitable for computing quantities for statistical analysis, such as averages and correlations. Statistical mechanics provides a framework to relate the microscopic properties of a system, such as particles, to the macroscopic properties, such as bulk flow. Assuming the dynamics occurs in statistical equilibrium, statistical mechanics is also a useful way to analyse the behavior of a system and to validate the numerical model. To derive meaningful statistical theory, the system in question should preserve volume and conserve certain quantities in its continuous form. However, it is not always clear whether a simulation of the system's discrete dynamics will retain the conservation properties of the continuous system. This will depend on the numerical method used, since the statistical mechanics resulting from a simulation are greatly affected by the choice of discretization and time integration. The effect of a method is to introduce a numerical bias, a change in the statistics of the continuum. In essence it is the statistics of the method, not the model, that we observe. Hence, it is important to develop methods whose statistics approximate that of the continuum as well as possible. It is the conservation laws of both continuum and method that drive the statistics.

For climate simulations, the surface of a sphere is an important domain to investigate due to its similarity to the shape of the earth. However, in developing computational methods to solve partial differential equations on a sphere, the topology of the spherical coordinate system leads to what is collectively known as the *pole problem*. These computational problems have largely been dealt with using the spectral method, based on spherical harmonics [32].

This thesis reports the results of implementing a numerical method, particularly suited for Hamiltonian fluid mechanics, to investigate its statistical properties when solving a classic, yet simple, geophysical model on a sphere. Specifically, we adapt the Hamiltonian Particle Mesh method [11] for the quasigeostrophic model on the sphere.

The text is organized as follows:

The remainder of chapter 1 will provide some background knowledge. In chapter 2, we introduce the quasigeostrophic model and in chapter 3, we explain the numerical method and its properties, as well as some properties of the spherical domain. In chapter 4 we present numerical results comparing energy conservation for both integration methods and discretization resolution, as well as exploring the statistics of our method and implementation. Chapter 5 briefly summarizes the results and suggestions for future work.

## 1.2 Models for geophysical flow

In modern day geophysical fluid flow theory the hierarchy of models relevant for atmospheric research, in decreasing complexity, are the three-dimensional Euler equations, the hydrostatic (primitive) equations (neglecting sound waves), the shallow water equations (2D) and the semi- and quasigeostrophic model (2D, without inertia-gravity waves). Each of these models represents a successive simplification of geophysical fluid flow, filtering out physical phenomena which are deemed unimportant contributors to the flow to be investigated[25]. Here we have chosen to investigate the quasigeostrophic (QG) model. Its structure is similar to the more sophisticated models and yet its statistics are relatively well understood, making it suitable for studying the statistical bias of numerical methods. In the following section we introduce some fundamental concepts for the analysis to come.

### 1.2.1 Hamiltonian systems

The geophysical fluid models listed above share a common mathematical structure, that of Hamiltonian systems, which is described in [14] as follows. Let $\boldsymbol{y} \in \mathbb{R}^N$. A finite-dimensional Hamiltonian system can be described by the equations

$$\dot{\boldsymbol{y}} = \boldsymbol{J}(\boldsymbol{y})\nabla H(\boldsymbol{y})$$

where $\boldsymbol{y}$ is the column vector of dynamical variables, $H$ is a Hamiltonian function, the energy of the system, and the *structure matrix* $\boldsymbol{J}$ is skew-symmetric and satisfies the Jacobi-identity

$$\sum_k (J_{lk}\partial_k J_{mn} + J_{nk}\partial_k J_{lm} + J_{mk}\partial_k J_{nl}) = 0, \qquad \forall l, m, n \leq N$$

where $N$ is the dimension of the system. If

$$\boldsymbol{J} = \begin{pmatrix} \boldsymbol{0} & \boldsymbol{I}_{N/2} \\ -\boldsymbol{I}_{N/2} & \boldsymbol{0} \end{pmatrix} \tag{1.2.1}$$

the system is called canonical, otherwise it is noncanonical, in particular if $\boldsymbol{J}$ is a singular matrix. If $\boldsymbol{J}$ is dependent on $\boldsymbol{y}$, the system is called a Poisson system.

We denote the *Poisson bracket* of functions $F(\boldsymbol{y}), G(\boldsymbol{y}) : \mathbb{R}^N \Rightarrow \mathbb{R}$ by

$$\{F, G\} = (\nabla F, \boldsymbol{J}\nabla G)$$

where $(\cdot, \cdot)$ denotes the scalar product of two vectors. Due to the skew-symmetry of $\boldsymbol{J}$ we have

$$\{F, G\} = -\{G, F\}.$$

If the Hamiltonian system is noncanonical, the Poisson bracket will be singular. The bracket can be seen as an abstract and geometric way to describe the system dynamics.

The time evolution of any function $F(\boldsymbol{y})$ along a solution to $\dot{\boldsymbol{y}} = \boldsymbol{J}(\boldsymbol{y})\nabla H(\boldsymbol{y})$ is given by the Lie derivative

$$\frac{dF}{dt} = (\nabla F, \dot{\boldsymbol{y}}) = (\nabla F, \boldsymbol{J}\nabla H) = \{F, H\},$$

i.e. the derivative of a function $F$ along a solution is given by its Poisson bracket with the Hamiltonian. For an ordinary differential equation $\dot{\boldsymbol{y}} = f(\boldsymbol{y})$, a nonconstant function $I(\boldsymbol{y})$ is called a *first integral* if $I(\boldsymbol{y}(t))$ is constant along any solution, i.e. if

$$\frac{d}{dt} I(\boldsymbol{y}(t)) = (\nabla I, \dot{\boldsymbol{y}}) = \{I, H\} = 0.$$

For $H$ itself, the skew-symmetry of the bracket implies

$$\frac{dH}{dt} = \{H, H\} = -\{H, H\} = 0$$

i.e. $H$ is a *conserved quantity* of the system.

First integrals can be of substantial physical and practical importance, as their level sets foliates the phase space. Numerically, they sometimes provide a simple way of distinguishing plausible trajectories from nonphysical ones, or of assessing the quality of an approximation [13].

Noncanonical Hamiltonian systems give rise to functions $C(\boldsymbol{y})$, called *Casimirs*, that vanish identically in the Poisson bracket with any other function $F$, i.e.

$$\{F, C\} = 0, \quad \forall F = F(\boldsymbol{y}) \quad \Leftrightarrow \quad \boldsymbol{J}\nabla C = 0.$$

Casimirs are obviously first integrals, and their existance is related to the singularity of $\boldsymbol{J}$.


**Symplectic structure**

Let $\dot{\boldsymbol{y}} = f(\boldsymbol{y})$ be an ordinary differential equation with the phase space $\mathbb{R}^N$. Define the flow over time $t$ as a mapping $\phi_t$ that advances the solution by time $t$, i.e. $\phi_t(\boldsymbol{y}_0) = \boldsymbol{y}(t, \boldsymbol{y}_0)$, where $\boldsymbol{y}(t, \boldsymbol{y}_0)$ is the solution of the system corresponding to the initial value $\boldsymbol{y}(0) = \boldsymbol{y}_0$. A smooth map $\phi_t$ on the phase space $\mathbb{R}^N$ is called a *symplectic map* with respect to the (constant and invertible) structure matrix $J$ if its Jacobian $\phi_t'(\boldsymbol{y})$ satisfies

$$\phi_t'(\boldsymbol{y})^T J^{-1} \phi_t'(\boldsymbol{y}) = J^{-1} \tag{1.2.2}$$

for all $\boldsymbol{y}$ in the range of $\phi_t$. If $J$ has the form of 1.2.1, then the $\phi_t$ is also called a 'canonical map'.

It is well known (see e.g. [13]) that the flow map $\phi_t$ of a Hamiltonian system is symplectic. In addition, symplectic maps are volume preserving, since by taking the determinant of (1.2.2) we get

$$|\phi_t'(\boldsymbol{y})|^2|J^{-1}| = |J^{-1}|,$$

for constant $J$, so either $|\phi_0'(\boldsymbol{y})|$ is +1 or -1. Since at $t = 0$, $|\phi_0'(\boldsymbol{y})| = 1$, we have that $|\phi_t'(\boldsymbol{y})| = 1$ for any $t$ by continuity, thus the volume is preserved under the symplectic mapping.

Similarly, we define a Poisson map to be the flow map of a Poisson system, satisfying

$$\phi_t'(\boldsymbol{y})^T J(\boldsymbol{y})\phi_t'(\boldsymbol{y}) = J(\phi(\boldsymbol{y})) \tag{1.2.3}$$

## 1.3  Geometric integrators

A dynamical system is characterized by its qualitative or *geometric* properties. Examples of such properties are the conservation of volume and the existence of first integrals, both of these describe the available phase space of the system. Geometric integrators are numerical methods that preserve geometric properties of the flow.

A one-step numerical method $\phi_h : \boldsymbol{y}^{n+1} = \phi_h(\boldsymbol{y}^n), t_{n+1} = t_n + \Delta t$, is called *symplectic* with respect to $J$ if the map $\boldsymbol{y}^n \mapsto \boldsymbol{y}^{n+1}$ is symplectic whenever the method is applied to a smooth Hamiltonian system.

Examples of symplectic methods are the symplectic Euler rule, the implicit midpoint rule, the Stormer-Verlet scheme, the Gauss collocation methods and certain Runge-Kutta methods.

Symplectic integrators do not generally conserve the Hamiltonian exactly, although they do so approximately (i.e. within bounded fluctuations with small amplitude). They do however conserve volume and some also preserve certain first integrals of a system, such as the implicit midpoint rule which preserves quadratic invariants of the form $I = \frac{1}{2}\boldsymbol{y}^T A \boldsymbol{y} + b^T \boldsymbol{y}$. Another way to preserve first integrals is via splitting methods [13].

Poisson integrators are symplectic integrators generalized to Poisson systems. A numerical method $\phi_h : \boldsymbol{y}^{n+1} = \phi_h(\boldsymbol{y}^n), t_{n+1} = t_n + \Delta t$ is called a Poisson integrator for the structure matrix $J(\boldsymbol{y})$ if the mapping $\boldsymbol{y}^n \Rightarrow \boldsymbol{y}^{n+1}$ preserves the Casimirs and is a Poisson map (1.2.3) when applied to a Poisson system.

## 1.4  Numerical discretization

Different numerical discretizations can result in very different discrete dynamics. Backward error analysis shows us that each distinct discretization is well approximated by a different modified differential equation with distinct

statistics. The choice of method can therefore greatly influence the statistical results obtained from simulations. In the context of the quasi-geostrophic model, this was made evident in [7], by showing that conservation properties of a discretization define the climatic mean of the dynamics. This result for one indicates that we must specify an appropriate criteria for what we want from a numerical discretization.

In order to achieve accurate statistical analysis from simulations, it is essential that the discretization conserves the quantities of interest which are conserved by the continuous system. Under the assumption of ergodicity, which is briefly introduced in Section 3.5, a dynamical system will sample its equilibrium distribution in phase space independent of its initial state. Its motion is constrained by its conservation laws. When the flow is volume preserving, the Poincaré recurrence theorem ensures that every neighborhood of all points in a compact invariant subspace is sampled repeatedly. Hence the conservation properties define the statistical behavior of the system.

The quasigeostrophic model's quantities of interest are, besides energy, all moments of potential vorticity. Thus the chosen discretization should conserve these quantities for statistical purposes. For fluids, Poisson structure is difficult to preserve in an Eulerian framework (see Section 1.4.1). One notable exception is the Zeitlin truncation [34], which retains Poisson structure and a finite approximation to the infinite class of Casimir invariants. The Zeitlin method however is limited to 2D incompressible flow with periodic boundary conditions. Other Eulerian methods fail to retain the Poisson structure or conserve the Casimirs in general. Most commonly preserved are quadratic invariants, which are limited to producing Gaussian statistics.

In trying to achieve proper conservation of structure, other discretization options include the point vortex method (see for example [4]), which is conservative yet simple, but has $O(K^2)$ complexity, where $K$ is the number of point vortices; and the Hamiltonian Particle Mesh method (HPM), a regularized point vortex method with potentially $O(K)$ complexity for $K$ particles. The HPM makes use of an Eulerian rectangular grid, $N_\lambda \times N_\theta$, where $N_\lambda \geq N_\theta$ and $N_\lambda^2 \sim K$. Furthermore, it uses a Lagrangian fluid description and conserves the desired quantities (see Section 1.4.1).

### 1.4.1  Lagrangian vs. Eulerian fluid discretization

The fluids study in the current geophysical context are composed of molecules, which can be regarded as point masses obeying Newton's laws of motion. In fluid mechanics, the most traditional general method to derive the equations governing macroscopic variables, like velocity, is to treat fluid as if it were a continuous distribution of mass in space [25]. The two common descriptions of continuum fluid motion are called Eulerian and Lagrangian. In the Eulerian description, the independent variables are the space coordinates $\boldsymbol{x} = (x, y, z)$ and time $t$. Dependent variables include the velocity, the mass

density and the pressure. The coordinate system represents a fixed frame of reference.

Lagrangian theory regards the fluid as a continuous field of particles. The independent variables are a set of *particle labels* $\boldsymbol{a} = (a, b, c)$, and the time $t$. In this description, a 'particle' represents a (possibly large) parcel or mass of fluid undergoing macroscopic motion. The dependent variables are the positions,

$$\boldsymbol{x}(\boldsymbol{a}, t) = (x(a, b, c, t), y(a, b, c, t), z(a, b, c, t))$$

and the velocities,

$$\boldsymbol{v}(\boldsymbol{a}, t) = \left( \frac{\partial x}{\partial t}, \frac{\partial y}{\partial t}, \frac{\partial z}{\partial t} \right)$$

at time $t$, of the fluid particle identified by $\boldsymbol{a}$. This particle label remains fixed as the fluid moves from place to place.

We will also later use the Lagrangian or *material* derivative, describing the evolution of a function $F$ of a certain fluid parcel in time. Seeing that the $t$-derivatives of the $(x, y, z)$ are the components of the velocity, $\boldsymbol{u} = \left( \frac{\partial x}{\partial t} \frac{\partial y}{\partial t} \frac{\partial z}{\partial t} \right)$, we obtain from the chain rule

$$\frac{dF}{dt} = \frac{\partial F}{\partial t} + u \frac{\partial F}{\partial x} + v \frac{\partial F}{\partial y} + w \frac{\partial F}{\partial z} = \frac{\partial F}{\partial t} + \boldsymbol{u} \cdot \nabla F.$$

## 1.5 Spherical harmonics

Enforcing the incompressibility constraint in certain geophysical fluid models frequently yields elliptic partial differential equations involving the Laplace (or Laplace-Beltrami) operator, the divergence of the gradient of a given function. Let $S^2 = \{(x, y, z) \in \mathbb{R}^3 : x^2 + y^2 + z^2 = a\}$ denote the 2-sphere with radius $a$. For functions on $S^2$, there exists a natural basis called the spherical harmonics. These functions are the eigenfunctions of the spherical Laplacian

$$\Delta f = \frac{1}{a^2 \sin \lambda} \frac{\partial}{\partial \lambda} \left( \sin \lambda \frac{\partial f}{\partial \lambda} \right) + \frac{1}{a^2 \sin^2 \lambda} \frac{\partial^2 f}{\partial \theta^2}$$

for a function $f$.

Let $l, m$ be integers such that $0 \le m \le l$ and let $\theta, \lambda$ be angles such that $0 \le \theta \le \pi$, $0 \le \lambda \le 2\pi$. Then the spherical harmonics are defined as [18]

$$Y_{l,m}(\lambda, \theta) = \left( \frac{(l-m)!(2l+1)}{4\pi(l+m)!} \right)^{1/2} e^{im\lambda} P_l^m(\cos \theta)$$

where $P_l^m(x)$ are the associated Legendre polynomials (see [18]) and the bracketed value is for normalization. $\theta$ and $\lambda$ are generally referred to as (co-)latitude and longitude.

Any function $f(\lambda, \theta) \in L^2(S^2)$ can be expanded in terms of the spherical harmonics

$$f(\lambda, \theta) = \sum_{l=0}^{\infty} \sum_{m=-l}^{l} f_l^m Y_l^m(\lambda, \theta)$$

To obtain numerical solutions, the expansion for $f$ must be truncated. It is shown [30] that this is an exponentially convergent approximation.

# Chapter 2

# The Quasi-Geostrophic Model

The dynamics of the atmosphere are governed by the Navier-Stokes equations, describing three dimensional, viscous and compressible fluid. For the purpose of study, a number of assumptions can be made to simplify the equations significantly. The main assumptions are those of inviscid fluid, incompressible flow and two dimensional flow.

Inviscid fluid flow is the assumption used to simplify the Navier-Stokes equations into the Euler equations, and is valid when viscous forces are negligible in comparison to inertial forces. Incompressibility is a reasonable assumption where wind speeds are less than approximately 1/3 the speed of sound, or about 300 km/hr.

One way to look at the two dimensional approach is to take note of the enormous difference in the horizontal and vertical scales of these fluid flows. Secondly, we must look into the behavioural difference between three dimensional and two dimensional turbulence. The direction of energy flow and the stability of solutions are important examples of the two behaving in opposite ways. It turns out that geophysical turbulence behaves much like two dimensional turbulence [3], strengthening the basis for the 2D approximation.

The quasigeostrophic equations are a simple model that meaningfully describes the motion of geophysical large scale flows [14] and it can adequately represent a single layer in a stratified flow. The vertical motion is dominated by the vertical pressure gradients, which is the hydrostatic balance. Following the hydrostatic assumption, the QG model is obtained through an asymptotic expansion of the Euler equations for fluid flow in the limit of a small Rossby number (see for example [19, 25] for the derivation). This leads to geostrophic balance, that is flow which is primarily governed by the balance of its horizontal pressure gradients and the Coriolis term [25]. Although full geostrophic balance rarely occurs, near-geostrophic balance is

a good approximation in regions outside of the tropics, thus for most areas
of the globe this approximation is considered justifiable.

The QG model does not include inertia-gravity waves, which makes it more
computationally tractable, since the fast movement of gravity waves imposes
strict time step limitations due to the CFL condition [25]. A small time step
requires more computing effort, making this a particularly important reason
for the model's popularity in the past.

## 2.1   The model and conserved quantities

The quasigeostrophic model is presented in various forms in the literature.
Here we consider a simple formulation of the model, called the 1.5 layer
quasi-geostrophic model.  It describes the vertical structure of the ocean
or the atmosphere in terms of an upper 'active' layer where the flow takes
place, and a lower layer, such as topography or stationary flow [3]. Bound-
ary conditions will be addressed later.

The quasigeostrophic potential vorticity equation describes barotropic divergence-
free flow over topography.  The full system is given by

$$\frac{d}{dt}q(\boldsymbol{x},t) = 0, \tag{2.1.1}$$

$$q = \Delta\psi - \frac{\psi}{R^2} + \eta_d \tag{2.1.2}$$

$$\boldsymbol{u} = \hat{\boldsymbol{k}}(\boldsymbol{x}) \times \nabla\psi \tag{2.1.3}$$

where $q$ is the potential vorticity, $\psi$ is the stream function and $\boldsymbol{u}$ is the
velocity field embedded in $\mathbb{R}^3$.  $\hat{\boldsymbol{k}}$ is the local unit normal vector on the
sphere at point $\boldsymbol{x}$, $\Delta$ is the Laplace-Beltrami operator and $\frac{d}{dt} = \frac{\partial}{\partial t} + \boldsymbol{u} \cdot \nabla$
is the material derivative.

$R$ is the Rossby deformation radius (not to be confused with the Rossby
number, see [3] or [25] for discussion), which can be estimated by dimensional
analysis as

$$R \sim \frac{\sqrt{gH}}{f}$$

where $g$ is the gravitational and centrifugal force, $f$ the Coriolis parameter
and $H$ is the thickness of the upper layer, here we use a mean value.  The
term $\psi/R^2$ describes the relationship between the gravitaional forces and
the stream function, and how it relates with the interface between the two
layers.  The term $\eta_d$ represents the effects of either topography or a given
stationary flow in the lower layer, which in a spherical setting is given by

$$\eta_d = \frac{\psi_d}{R^2},$$

as in [3], without the beta-plane effect. $\psi_d$ is a stream function that "induces a permanent deformation of the interface with respect to its horizontal position" [3]. Thus, for the active layer the deep flow represents topography, which is frequently explicitly stated in other versions of the QG model [14, 25].

In general, $\psi$ is called the stream function because at any fixed instant in time the velocity field $\boldsymbol{u}$ is perpendicular to the gradient of $\psi$, i.e. $\boldsymbol{u}$ is tangent to the level curves of $\psi$. Therefore the level curves of $\psi$ represent the streamlines of the fluid, which in a steady flow are the trajectories of the fluid particles. Furthermore, physically, $\psi$ represents the hydrostatic pressure of the fluid. From the velocity field, $\boldsymbol{u} = \hat{\boldsymbol{k}}(\boldsymbol{x}) \times \nabla\psi$, it follows that the streamlines are also the isobars of the flow. Thus in a steady state solution, the fluid flows along isobars instead of going from high pressure regions to low pressure regions as it the situation for non-rotating fluids [14].

The quasi-geostrophic model describes a Hamiltonian system, with the Hamiltonian

$$\mathcal{H} = -\frac{1}{2}\int_{S^2} \psi(q - \eta_d) \tag{2.1.4}$$

where $S^2$ is the surface of a unit sphere. It can be shown that this Hamiltonian is a conserved quantity. Other conserved quantities are most prominently the generalized potential enstrophies $\mathcal{G} = \int_{S^2} G(q)$ for all $G$ [14] as follows:

$$\frac{d\mathcal{G}}{dt} = \int G'(q)\nabla q \cdot \nabla^\perp \psi \, dx = \int \nabla \cdot \left( G(q)\nabla^\perp \psi \right) \, dx = 0$$

by Gauss's theorem and periodic boundary conditions. Due to the spherical geometry, the angular momentum is also conserved.

## 2.2 The QG model on a sphere

In [14] the quasi-geostrophic equations have been studied extensively, particularly in flat, two-dimensional geometry, using the beta-plane approximation. By extending the methodology of [8], the focus here is on the statistics of numerical methods on the sphere. As such, this work can be seen as a combined approach based on [8] and [10].

In [14], the beta-plane two-dimensional model is the main focus, while the spherical model is introduced in the final chapter. Partly this is due to the many similar properties of the two. Furthermore, although the planar case needs the additional beta-plane term, the geometry is much simpler to work with than the spherical one. However, rigorous global theory about the sphere is available and has been for many years [27, 33].

The study of geophysical flows on the sphere is of obvious importance due to the spherical geometry of the earth and other planets. Most of the phenomena present on the sphere have their counterpart in flat geometry. However, certain features are unique to the sphere due to the special geometry, one being the natural periodic boundary. In fact, the symmetry of the spherical domain gives rise to more conservation laws [25], but the study of these is left for future work.

# Chapter 3

# The HPM Method

The Hamiltonian Particle Mesh method is a numerical discretization for advecting particle flow first proposed for the rotating shallow water equations in [11]. It uses a Lagrangian description of inviscid fluid flow and retains Hamiltonian structure, as well as conserving energy up to bounded fluctuations on long time intervals. The fluid flow is coupled to an Eulerian longitude-colatitude grid for evaluating derivatives. Applied to the QG model, the HPM method can be viewed as a regularized point vortex method [8].

The fluid is discretized via the potential vorticity field, $q$, by introducing a set of $K$ particles each with a fixed potential vorticity $Q_k, k = 1, \ldots, K$. These particles have a time dependent position $\boldsymbol{X}_k(t)$ and they are advected in a divergence free velocity field according to

$$\frac{d}{dt}\boldsymbol{X}_k = \boldsymbol{X}_k \times \nabla\Psi(\boldsymbol{x}, t)\mid_{\boldsymbol{x}=\boldsymbol{X}_k(t)}. \tag{3.0.1}$$

Here $\Psi$ is the continuous interpolation of a given discrete grid-based stream function. Let $\boldsymbol{i} = (i_1, i_2)$ denote a gridpoint on the colatitude-longitude grid. The continuous stream function is constructed by

$$\Psi(\boldsymbol{x}, t) = \sum_{\boldsymbol{i}} \Psi_{\boldsymbol{i}}(t)\phi_{\boldsymbol{i}}(\boldsymbol{x}) \tag{3.0.2}$$

where $\phi_{\boldsymbol{i}}$ is a basis function to be defined later.

The discrete stream function $\Psi_{\boldsymbol{i}}(t)$ is obtained by solving a Helmholtz equation, equation (2.1.3), on the grid. Given a discrete grid-based potential vorticity field $q_{\boldsymbol{i}}(t)$ we solve

$$\sum_{\boldsymbol{j}}(\Delta_{\boldsymbol{ij}} - R^{-2})\Psi_{\boldsymbol{j}} = q_{\boldsymbol{i}} - \eta_{d_{\boldsymbol{i}}} \tag{3.0.3}$$

for $\Psi_{\boldsymbol{j}}$, where $\eta_{d_{\boldsymbol{i}}}$ encompasses the lower layer, or the topography on the grid, and $\Delta_{\boldsymbol{ij}}$ is an appropriate discretization of the Laplacian. To solve the

elliptic equation on the discrete grid we use a spherical solver (see below). The discretized potential vorticity field on the grid is approximated from the particle positions using

$$q_{\boldsymbol{i}}(t) = \sum_k Q_k \phi_{\boldsymbol{i}}(\boldsymbol{X}_k(t)). \tag{3.0.4}$$

Here the basis functions $\phi_{\boldsymbol{i}}$ play a dual role as smooth kernel functions satisfying a partition of unity, $\int \phi_{\boldsymbol{i}}(x) d\lambda d\theta = 1$.

## 3.1  Spherical discretization

Since the intention of this research is to implement a spherical model, the aforementioned Eulerian grid is a longitude-colatitude grid of size $\pi \times 2\pi$ in terms of $N_\theta \times N_\lambda$ grid points with uniform spacing in both direction, $\Delta\theta = \pi/(N_\theta - 1)$ and $\Delta\lambda = 2\pi/N_\lambda$. A single grid point is denoted $(\lambda_m, \theta_n)$, where $\lambda_m = m\Delta\lambda, \quad \theta_n = n\Delta\theta$, for $m = 0, \ldots, N_\lambda - 1$ and $n = 0, \ldots, N_\theta$, largely following [10]. Then, $\lambda \in [0, 2\pi]$ and $\theta \in [0, \pi]$, where $\theta_0$ corresponds to the North pole, complying with the spherical solver (see next section). All particle positions $\boldsymbol{X}_k$ are constrained to the surface of the sphere,

$$\boldsymbol{X}_k \cdot \boldsymbol{X}_k = a^2 \tag{3.1.1}$$

where $a > 0$ is the radius of the sphere. The conversions between Cartesian and spherical coordinates follow the formulas

$$x = a \sin\theta \cos\lambda, \quad y = a \sin\theta \sin\lambda, \quad z = a \cos\theta$$

and

$$\lambda = \tan^{-1}(y/x), \quad \theta = \cos^{-1}(z/a)$$

Thus each particle position $\boldsymbol{X}_k = (x_k, y_k, z_k)$ is associated with a spherical coordinate $(\lambda_k, \theta_k)$.

To compute $\nabla\psi$ to later establish the velocity field, we use the gradient in $\mathbb{R}^3$

$$\nabla_{\boldsymbol{x}} = \left( \frac{\partial}{\partial x}, \frac{\partial}{\partial y}, \frac{\partial}{\partial z} \right)$$

Then by applying the chain rule we obtain

$$\nabla_{\boldsymbol{x}} = \frac{1}{a} \hat{\boldsymbol{\theta}} \frac{\partial}{\partial \theta} + \frac{1}{a \sin\theta} \hat{\boldsymbol{\lambda}} \frac{\partial}{\partial \lambda}$$

where

$$\hat{\boldsymbol{\theta}} = (\cos\lambda\cos\theta, \sin\lambda\cos\theta, \sin\theta)^T$$

$$\hat{\boldsymbol{\lambda}} = (-\sin\lambda, \cos\lambda, 0)^T$$

are unit vectors in spherical coordinates.

### 3.1.1   Basis functions

The basis functions $\phi_{\boldsymbol{i}}(\boldsymbol{x})$ on the sphere are implemented using cubic spline functions defined on a colatitude-longitude grid $(\lambda_{i1}, \theta_{i2})$. $\phi$ is a compactly supported basis function satisfying symmetry, normalization and partition of unity in the following sense:

$$\phi(\boldsymbol{x}) = \phi(-\boldsymbol{x}), \quad \int_{\mathbb{R}^2} \phi(\boldsymbol{x})d\lambda d\theta = 1, \quad \sum_i \phi_{\boldsymbol{i}}(\boldsymbol{x}) = 1, \quad \forall \boldsymbol{x} \in S^2.$$

A particle position $\boldsymbol{X}_k \in \mathbb{R}^3$ is mapped to the grid according to a mapping $\eta$: $(\lambda_k, \theta_k) = \eta(\boldsymbol{X}_k)$. We define the basis function for $i_2 \geq 2$ and $i_2 \leq N_\theta - 2$ as

$$\phi_{\mathbf{i}}(\boldsymbol{X}_k) = \tilde{\phi}\left(\frac{\lambda_k - \lambda_{i_1}}{\Delta\lambda}\right)\tilde{\phi}\left(\frac{\theta_k - \theta_{i_2}}{\Delta\theta}\right)$$

where $\tilde{\phi}$ is the cubic B-spline basis function:

$$\tilde{\phi}(r) = \begin{cases} \frac{2}{3} - |r|^2 + \frac{1}{2}|r|^3, & |r| \leq 1, \\ \frac{1}{6}(2 - |r|)^3, & 1 < |r| \leq 2, \\ 0, & \text{otherwise.} \end{cases}$$

In the neighborhood of the pole the basis functions are modified as follows:

- The polar basis function is a function of $\theta$ only:

$$\phi_0(\boldsymbol{X}_k) = \tilde{\phi}\left(\frac{\theta_k - 0}{\Delta\theta}\right)$$

$$\phi_\pi(\boldsymbol{X}_k) = \tilde{\phi}\left(\frac{\theta_k - \pi}{\Delta\theta}\right)$$

- The basis functions once removed from the pole have global support in the longitudinal direction

$$\phi_{\mathbf{i}}(\boldsymbol{X}_k) = \kappa\tilde{\phi}\left(\frac{\lambda_k - \lambda_{i_1}}{\pi}\right)\tilde{\phi}\left(\frac{\theta_k - \theta_{i_2}}{\Delta\theta}\right)$$

where the scaling constant $\kappa$ is determined such that the normalization

$$\int \phi_{\mathbf{i}}(\boldsymbol{x})d\lambda d\theta = 1$$

is maintained.

## 3.2    Spherical harmonics

To solve the QG model's Helmholtz equation (2.1.3), we use Spherepack
3.0, a robust collection of Fortran programs developed by the U.S. National
Center for Atmospheric Research, designed for the development of com-
puter models of geophysical processes [1]. Spherepack employs the spectral
method, meaning essentially that scalar and vector harmonic analyses are
used in spherical coordinates in the same way that Fourier analysis is used
on the plane in Cartesian coordinates.  Spectral methods are also called
global methods, since each point interacts with all the other points on the
sphere [32].  Thus, a key benefit of the spectral method, and the reason
for its popularity are its exponential convergence rate and isotropy on the
sphere, avoiding the pole problem.
The uniformity of the spectral method ensures that the large number of grid
points located near the pole, due to the coordinate system, does not create
computational instabilities by being 'oversampled'. The effect is to smooth
the original function by sampling evenly in terms of Cartesian coordinates
rather than spherical [29].

For spherical geometry, the spherical harmonics form a natural basis; an
orthogonal basis that is isotropic on the sphere.  This means that using
spherical harmonics to solve partial differential equations will lead to uniform
accuracy independent of the location on the sphere.
As hinted in section (1.5) a truncated expression of a function $f(\lambda, \theta) \in L^2$
to $N$ modes can be formulated like this:

$$f(\lambda, \theta) = \sum_{n=0}^{N} {\sum_{m=0}^{n}}' \hat{f}_{n,m} \bar{Y}_n^m(\lambda, \theta)$$

for coefficients $\hat{f}_{m,n}$, where $\bar{Y}_n^m$ is defined as before. Let the spherical inner
product of two functions $f(\lambda, \theta), g(\lambda, \theta)$ be defined by:

$$\langle f, g \rangle = \int f(\lambda, \theta) g^*(\lambda, \theta) \sin \theta d\theta d\lambda$$

where $*$ denotes the adjoint operator.  The spherical harmonic basis function
are orthogonal in the sense that

$$\left\langle Y_l^m, Y_{l'}^{m'} \right\rangle = \delta_{ll'} \delta_{mm'}.$$

Given a discrete function on a colatitude-longitude grid of dimension $N_\lambda \times N_\theta$
where $N_\lambda = 2(N_\theta - 1)$ and $\Delta \theta = \Delta \lambda$, we want to expand that function in
terms of the spherical harmonic basis.  Swarztrauber [29] reviews a num-
ber of methods to implement the discrete transform.  All methods have in
common that they apply a discrete Fourier transform in the longitudinal

direction.

Let $F$ denote the dicrete Fourier transform matrix. Then $F^*F = I$, the identity matrix on $\mathbb{R}^{N_\lambda \cdot N_\theta}$. The $*$ denotes the conjugate transpose. Let $P$ denote the matrix that performs the discrete synthesis in associated Legendre polynomials. Then, given the expansion coefficients $\hat{f} = (\hat{f}_{m,n})$, the synthesis

$$f = F^*P\hat{f}$$

exactly evaluates the spherical harmonic expansion at all grid points $vecti$:

$$f_{\boldsymbol{i}} = \sum_{m,n} \hat{f}_{m,n} Y_n^m(\lambda_{i_1}, \theta_{i_2})$$

The methods in [29] differ in how they compute the spectral analysis. A general approach is to first perform a Fourier transform in the longitudinal direction, and then to evaluate inner products with associated Legendre polynomials using quadrature. We represent the spectral analysis in matrix form as follows:

$$\hat{f} = ZFf$$

where $f = (f_{\boldsymbol{i}})$ is a grid function, and $Z$ represents the quadrature weights. For the particular case of Neumann's method [9], one has $Z = P^*$, and $ZZ^* = I_N$ on the spherical harmonic space. ($Z^*Z$ is not the identity on $\mathbb{R}^{N_\lambda \cdot N_\theta}$ however).

Let $\mathcal{S}$ be the set of $L^2$ functions which can be expanded in spherical harmonics. If $f, g \in \mathcal{S}$, it can be shown that

$$\langle f, g \rangle = \sum_{m,n} \hat{f}_{m,n}^* \hat{g}_{m,n},$$

the sum of the spherical harmonics expansion coefficients.

The Hamiltonian (2.1.4) for the QG system is:

$$H = \frac{1}{2} \langle \psi, q - \eta_d \rangle$$

where $\psi = (\Delta - R^{-2})^{-1}(q - \eta_d)$ is established using the spectral method, resulting in expansion coefficients $\hat{\psi}_{m,n} = (\hat{q}_{m,n} - \hat{\eta}_{d_{m,n}})/(m(m+1) + R^{-2})$. In terms of spherical harmonics expansion, this becomes:

$$H = \frac{1}{2} \sum_{m,n} \frac{|\hat{q}_{m,n} - \hat{\eta}_{d_{m,n}}|^2}{m(m+1) + R^{-2}}. \tag{3.2.1}$$

Using Neumann's method, we proceed as follows. Given the vorticity field $q = (q_{\boldsymbol{i}})$ on the grid, we first project this field onto the space of grid functions $\mathcal{S}$, that may be exactly represented (interpolated) by the spherical harmonics

basis. We define a projection operator consisting of an analysis followed immediately by a synthesis:

$$\mathbb{P} = F^* PZF$$

and construct the function $\tilde{q} := \mathbb{P}q$, then $\tilde{q} \in \mathcal{S}$. Next we apply the analysis to get $\hat{q} := ZF\tilde{q}$.

The Hamiltonian is as in equation (3.2.1) and the particle dynamics are defined by

$$Q_k \dot{\boldsymbol{X}}_k = \boldsymbol{X}_k \times \frac{\partial H}{\partial \boldsymbol{X}_k} \qquad (3.2.2)$$

for a particle $k$, thus describing a Poisson system. This Hamiltonian structure is equivalent to that of point-vortex dynamics, generalized to the sphere in [17]. Note that for any point $\boldsymbol{x}$, the velocity field should satisfy

$$U(\boldsymbol{x}) = \hat{\boldsymbol{k}}(\boldsymbol{x}) \times \nabla \psi$$

where $\psi$ is the stream function, and $\hat{\boldsymbol{k}}(\boldsymbol{x})$ is the local unit normal vector at point $\boldsymbol{x}$ on the sphere: $\hat{\boldsymbol{k}}(\boldsymbol{x}) = \boldsymbol{x}/|\boldsymbol{x}|$, i.e. the normalized particle position. We assume $|\boldsymbol{x}| = 1$. Hence we would like to see that for a particle $k$,

$$\frac{\partial H}{\partial \boldsymbol{X}_k} \approx Q_k \nabla \psi(\boldsymbol{X}_k)$$

for consistency. Conservation of energy is implied by (3.2.2), since

$$\sum_k \frac{\partial H}{\partial \boldsymbol{X}_k} \frac{d\boldsymbol{X}_k}{dt} = \sum_k \frac{\partial H}{\partial \boldsymbol{X}_k} \cdot \left( \frac{\boldsymbol{X}_k}{Q_k} \times \frac{\partial H}{\partial \boldsymbol{X}_k} \right) = 0$$

by skew symmetry of the cross product. We apply the chain rule to compute

$$\frac{\partial H}{\partial \boldsymbol{X}_k} = \sum_{m,n,\boldsymbol{i},\boldsymbol{j}} \frac{\partial H}{\partial \hat{q}_{m,n}} \cdot \frac{\partial \hat{q}_{m,n}}{\partial \tilde{q}_{\boldsymbol{i}}} \cdot \frac{\partial \tilde{q}_{\boldsymbol{i}}}{\partial q_{\boldsymbol{j}}} \frac{\partial q_{\boldsymbol{j}}}{\partial \boldsymbol{X}_k}$$

$$= \sum_{m,n,\boldsymbol{i},\boldsymbol{j}} \hat{\psi}_{m,n} (ZF)_{\boldsymbol{i}}^{m,n} \mathbb{P}_{\boldsymbol{j}}^{\boldsymbol{i}} \frac{\partial q_{\boldsymbol{j}}}{\partial \boldsymbol{X}_k}$$

where $\partial q_{\boldsymbol{j}}/\partial \boldsymbol{X}_k = Q_k \phi'_{\boldsymbol{j}}(\boldsymbol{X}_k)$. In matrix form:

$$\frac{\partial H}{\partial \boldsymbol{X}} = \frac{\partial H}{\partial \hat{q}} \cdot \frac{\partial \hat{q}}{\partial \tilde{q}} \cdot \frac{\partial \tilde{q}}{\partial q} \cdot \frac{\partial q}{\partial \boldsymbol{X}}$$

$$= \hat{\psi} \cdot ZF\mathbb{P} \frac{\partial q}{\partial \boldsymbol{X}}$$

$$= (\mathbb{P}^* (ZF)^* \hat{\psi}) \cdot \frac{\partial q}{\partial \boldsymbol{X}}$$

$$= F^* Z^* P^* F F^* Z^* \hat{\psi} \cdot \frac{\partial q}{\partial \boldsymbol{X}}$$

$$= F^* Z^* P^* Z^* \hat{\psi} \cdot \frac{\partial q}{\partial \boldsymbol{X}}$$

For the method of Neumann, the following steps are

$$= F^* P P^* P \hat{\psi} \frac{\partial q}{\partial \boldsymbol{X}}$$

$$= F^* P \hat{\psi} \cdot \frac{\partial q}{\partial \boldsymbol{X}}$$

$$= \psi \cdot \frac{\partial q}{\partial \boldsymbol{X}}$$

or

$$\frac{\partial H}{\partial \boldsymbol{X}_k} = Q_k \sum_i \psi_i \phi_i'(\boldsymbol{X}_k)$$

as desired.

For the method of Machenauer and Daley, which is encoded in Spherepack, we have the identity $ZP = I_N = P^* Z^*$, and the above relation becomes:

$$\frac{\partial H}{\partial \boldsymbol{X}} = F^* Z^* \hat{\psi} \cdot \frac{\partial q}{\partial \boldsymbol{X}}$$

where $ZF$ is a spherical harmonic analysis. However, Spherepack does not include a function for computing the adjoint operation. For numerical computation, we instead make the approximation $F^* Z^* \approx F^* P$ which will break exact energy conservation. We note that the exponential accuracy of the spherical harmonics approximation implies that the errors made here are relatively small.

Alternatives to this approximation include:

- implementation of Neumann's method

- implementation of the adjoint operation to the Spherepack analysis

We will check numerically that the energy is still sufficiently conserved.

## 3.3 Complexity, validation, verification

In terms of computational complexity, the spectral transform method called by Spherepack is the most intensive process of our implementation since it requires $O(N^3)$ operations for $N$ latitudinal grid points. Let $K$ denote the number of particles, and note that $K \sim N^2$. By using multigrid methods, instead of spherical harmonic analysis, the HPM complexity could in theory be reduced to $O(N^2)$. In comparison, the point vortex method [4] for $K$ point vortices is $O(K^2) = O(N^4)$. Despite the high complexity, Spherepack was chosen for this implementation due to its robustness and availability. Results from previous work using the HPM method on the sphere were published in [10] where the method is validated for a test case of the shallow

water equations.  The nonisotropic method of Merilees [10] was combined
with a regularization and shifted pole to avoid the polar problem, making
this combination of the HPM with the spectral method a new approach,
which could be developed and tested further.  By using a fully spectral
approach for this problem, only quadratic invariants would be preserved,
implying Gaussian statistics, whereas the HPM has been shown the plane to
be able to reproduce richer statistics. In terms of the QG model, statistical
theory on the plane was numerically verified in terms of the time averaged
relationship between $q$ and $\psi$ in [8]. Here we show similar results, where the
mean fields $\bar{q}$ and $\bar{\psi}$ have a linear relationship, as addressed in Section 3.5
on the validation of statistical theory.

## 3.4    Time integration

A numerical integrator for a long time simulation must be chosen with care
to fit the objectives of the research. For statistical analysis it is desirable to
fully exploit the conservation properties of both the model and the numer-
ical discretization method. We have already seen that energy should be a
conserved quantity throughout, at least approximately.
For our spherical surface embedded in $\mathbb{R}^3$, it is essential for the time inte-
gration that the particles remain on the sphere throughout the simulation.
For this to be fulfilled the norm of the particle position vectors should stay
equal to the sphere's radius. From (3.2.2) we have that

$$\frac{d}{dt}\|\boldsymbol{X}_k\|^2 = 2\boldsymbol{X}_k \cdot \frac{d\boldsymbol{X}_k}{dt} = 2\boldsymbol{X}_k \cdot \boldsymbol{X}_k \times \frac{\partial H}{\partial \boldsymbol{X}_k} = 0$$

following from skew-symmetry of the cross product. Thus the invariance of
the sphere is a Casimir of the Hamiltonian structure. We consider a number
of approaches for preserving this invariant.

1. **Projection:** We integrate the system $\dot{\boldsymbol{X}} = f(\boldsymbol{X})$ in time using a
   preferably high order explicit method (such as a 4th order Runge-
   Kutta method) and renormalize the particle positions after each time
   step. Let $\boldsymbol{X}^n$ denote positions at time $t = n\Delta t$. Then

$$\boldsymbol{X}^n \to \tilde{\boldsymbol{X}}^{n+1} \text{ (Runge-Kutta step)}$$

$$\boldsymbol{X}_k^{n+1} = \frac{\boldsymbol{X}_k^{\tilde{n+1}}}{\|\tilde{\boldsymbol{X}}_k^{n+1}\|} \text{ (renormalization)}$$

2. **Implicit midpoint:** The particle norm is a quadratic invariant in $\boldsymbol{X}$,
   and is automatically preserved by any Gauss-Legendre Runge-Kutta
   method. We use the implicit midpoint rule:

$$\boldsymbol{X}^{n+1} = \boldsymbol{X}^n + \Delta t f(\frac{\boldsymbol{X}^n + \boldsymbol{X}^{n+1}}{2})$$

The implicit midpoint method is a second order accurate, symplectic method, but is not a Poisson map for this problem.

3. **Rodriguez' formula:** Given a differential equation in $\mathbb{R}^3$: $\dot{z} = z \times a$, for a constant vector $a$, the exact solution is

$$z(t) = \exp(-t\hat{a})z(0),$$

where

$$\hat{a} = \begin{pmatrix} 0 & -a_3 & a_2 \\ a_3 & 0 & -a_1 \\ -a_2 & a_1 & 0 \end{pmatrix}$$

This is the mapping from the Lie algebra $\mathfrak{so}(3)$ to the Lie group $SO(3)$, the rotation group for 3-dimensional Euclidean space. An efficient implementation of the exponential can be achieved as follows:

$$\exp(\hat{a}) = I + \frac{\sin(At)}{A}\hat{a} + 2\left[\frac{\sin At/2}{A}\right]\hat{a}^2$$

where $A = \sqrt{a_1^2 + a_2^2 + a_3^2}$.

We approximate $\left(\frac{\partial H}{\partial \boldsymbol{X}_k}\right)^{n+1/2}$ at the midpoint $t_n + \Delta t/2$ using our method of choice. Then we apply the rotation according to

$$\boldsymbol{X}_k^{n+1} = \exp\left(-\tau\left(\frac{\partial H}{\partial \boldsymbol{X}_k}\right)^{n+1/2}\right)\boldsymbol{X}_k^n$$

In the next section we compare all three of the above methods in terms of energy drift.

## 3.5   Statistical theory and numerical validation

In addition to energy conservation, we wish to explore long time averages in terms of prior vorticity distributions, as in [7, 8]. To apply statistical theory, as introduced there we need to assume that the discrete dynamics are ergodic. We define the time average of a quantity $F(\boldsymbol{q}(t))$ to be

$$\bar{F}_T = \frac{1}{T}\int_{t_0}^{t_0+T} F(\boldsymbol{q}(t))dt$$

and the ensemble average to be

$$\langle F(\boldsymbol{q})\rangle = \int F(\boldsymbol{q})p(\boldsymbol{q})d\boldsymbol{q}$$

If the discrete dynamics are ergodic with respect to a unique invariant measure $p(\boldsymbol{q})$ on the phase space, then the long time average is equivalent to the

ensemble average with respect to $p$, $\langle F(\boldsymbol{q}) \rangle$.

The mean field statistical theory of 2D incompressible fluids is well developed [5, 12, 16, 21, 22, 26], see [14] and [3] for reviews.

For the special case of pointwise normally distributed potential vorticity $q$, we expect an equilibrium probability distribution on the space of potential vorticity fields:

$$p(q) \propto \exp\left(-\beta H(q)\right) - \alpha Z(q)$$

where $\beta$ and $\alpha$ play the role of Lagrange multipliers and $Z(q)$ is the quadratic enstrophy $Z = \int q^2 dx$. In this case, the most likely mean state satisfies

$$\langle -\beta \nabla H - \alpha \nabla Z \rangle = 0$$

so

$$-\beta \langle \psi \rangle - \alpha \langle q \rangle = 0$$

or

$$\langle q \rangle = \mu \langle \psi \rangle, \quad \mu = -\beta/\alpha.$$

Hence we expect the mean field to be pointwise linearly related. Furthermore, letting $R = \infty$ in equation (2.1.3), then in terms of the mean field problem $\Delta \langle \psi \rangle = \langle q \rangle - \eta_d$, we have the Helmholtz problem

$$(\mu - \Delta) \langle \psi \rangle = \eta_d \tag{3.5.1}$$

for the mean stream function. We validate our simulations with this theoretical $\langle \psi \rangle$ and the linear relation $\langle \psi \rangle = \mu \langle \psi \rangle$.

In our computations we measure the time averages of the potential vorticity and the stream function. Our results are roughly in line with the theory derived in [8], showing a linear relationship between $\langle q \rangle$ and $\langle \psi \rangle$ for Gaussian initial conditions. Detailed statistical theory for this problem is not derived here and is left for future work.

# Chapter 4

# Numerical results

The primary objectives of the numerical experimentation are to show that the implementation conserves energy and that the predicted mean field relation between $\langle q \rangle$ and $\langle \psi \rangle$ in [8] is reproduced.

## 4.1 Experimental setup

We choose $K$, the number of particles to be related to the grid resolution via $K = 2N_\lambda^2$.

All computations were performed in MATLAB, using its *mex* extensions for C, also for the Spherepack code which was adapted from Fortran to C. For the topography, $\eta_d$, we used the earth's topological data available in MATLAB, 'topo.dat', and adjusted it to scale with our computations which are performed on a unit sphere, i.e. with 1km radius. The small scale of the topography, compared to the size of the sphere, means that the scale of the potential vorticity, $q$, should be small as well, or somewhat comparable. This in turn allows us to use a relatively large time step and yet maintain a stable energy drift.

### 4.1.1 Energy conservation, based on the spatial discretization

The initial condition for our simulations is a combined approach of a predetermined equilibrium and a Gaussian distribution.

We initialize potential vorticity by choosing the slope $\mu = -0.732$ of the prospective equilibrium, $\langle q \rangle = \mu \langle \psi \rangle$ as done in [7]. To establish this we solve equation (3.5.1) on the grid and then set $q_{\boldsymbol{i}} = \mu \psi_{\boldsymbol{i}}$. The grid potential vorticity values are interpolated to the particle positions using the basis functions, and the energy computed, call it $H_0$. The particle values are replaced by normally distributed values with the same standard deviation, which are then randomly permuted to obtain the set of initial PV values
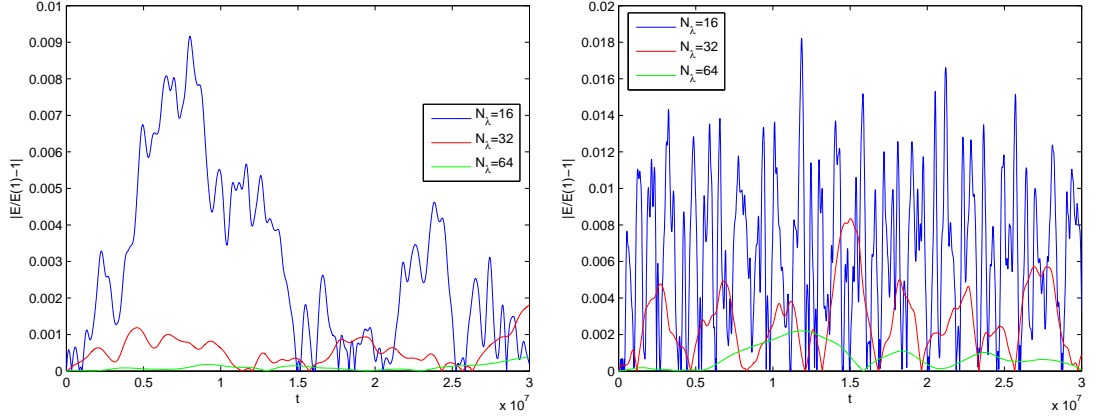
Figure 4.1: Energy drift with spatial discretization $N_\lambda = \{16, 32, 64\}$ and 4th order Runge-Kutta. $\Delta t = 10^5/N_\lambda$ and $T = 3 \times 10^7$. Left: $R = 1000/6371$. Right: $R = \infty$.

$\{Q_k\}$ using a Monte Carlo simulation, such that the energy, $H$, satisfies $|H - H_0| < 0.3 * |H_0|$.

For this analysis we take a rather large time step by setting $\Delta t = 10^5/N_\lambda$ and $T = 10^7$ for $N_\lambda = \{16, 32, 64\}$ and use the 4th order Runge-Kutta method. The results can be seen in figure 4.1 where we show the relative absolute drift of the energy,

$$\left| \frac{E - E(1)}{E(1)} \right|,$$

where $E(1)$ is the energy value at the beginning of the simulation.

We observe a dramatic difference by halving the spatial discretization twice. When $N_\lambda = 32, 64$ the drift stays at $O(10^{-3})$ and is in fact also within $O(10^{-2})$ for $N_\lambda = 16$. Another observation is how the fluctuations are up to four times larger when $R = \infty$, for all spatial resolutions, indicating that the 1.5 layer model is stabler than the single layer model, at least in terms of energy conservation. It should be noted that since $\Delta t$ is chosen to be resolution dependant, the time step goes down with higher resolution in these graphs. However, as seen in figure 4.2, we observe a only a very slow and limited convergence with a smaller time step, which is a drawback of the approximated energy and calls for future attention.

### 4.1.2   Energy conservation, based on the time integrator

Using the same initial condition as before, and the spatial discretization $N_\lambda \times N_\theta = 32 \times 17$ we let the time step be $\Delta t = 10^5/N_\lambda$ as before and
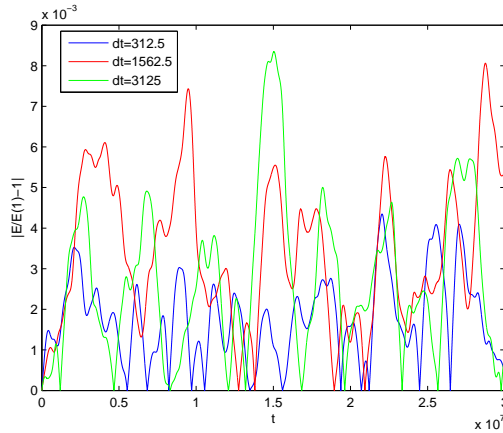
Figure 4.2: Energy drift with $N_\lambda = 32$, $\Delta t = \{10^5/N_\lambda, 5 \times 10^4/N_\lambda, 10^4/N_\lambda\}$, $R = \infty$ and 4th order Runge-Kutta with projection. The smallest time step results in drift approximately half the size of the other two.

compare the outcome of different time integrators; Runge-Kutta with projection, RK with rotation and the implicit midpoint method.The implicit midpoint nonlinear relations are resolved to maching precision.

The integrator comparison does not indicate a very large difference, taking a smaller time step yields a similar result in the long term. Again we see more volatility with $R = \infty$.

### 4.1.3 Statistical simulation

The mean field theory presented in [14] and introduced in Section 3.5, predicts a linear relationship between the potential vorticity and stream function mean fields. In light of the expected conservation of $q$, this is clear for the initial condition presented in the previous two sections, but is also shown to be the case for normally distributed initial values for $Q_k$.

The time integrations are computed for a time interval $[0, t_0 + T]$, where $t_0$ is the time required for the solution to decorrelated from the initial conditions. We take $N_\lambda = 16$, and set the time step to $\Delta t = 100$, $t_0 = 10^6$ and $T = 10^8$, using the 4th order Runge-Kutta method with projection. We use both the initial condition with a preset equilibrium slope as described above, as well as simply drawing the initial potential vorticity of the particles from the normal distribution with zero mean and standard deviation 0.001, and randomly permuting until the energy is computed to be $2^{-8} \pm 10\%$. The small standard deviation is chosen so that the potential vorticity field scales with the topography.

We note that since the former initial condition is based on the relationship
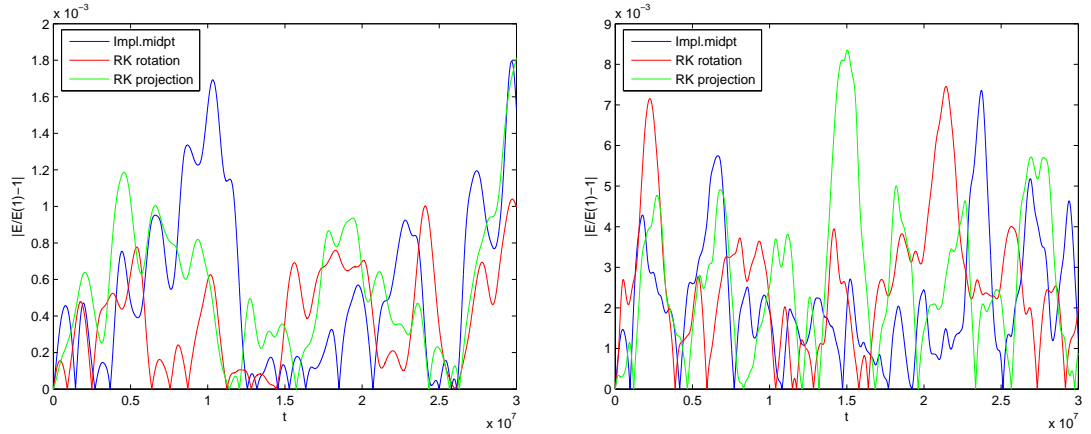
Figure 4.3: Energy drift with $N_\lambda = 32$ and $\Delta t = 10^5/N_\lambda$. Time integrators compared: projected 4th order Runge-Kutta, implicit midpoint rule and RK4 with rotation. Left: $R = 1000/6371$. Right: $R = \infty$.

$\Delta\psi = q - \eta_d$, i.e. with $R = \infty$, (see [7]), the predicted meanfield is only established for that case.

Figure 4.4 shows the locus $(\bar{q}_i, \bar{\psi}_i)$ for the two initial conditions plotted with $\mu = -0.732$ on one hand and a linear fit on the other. The initialized slope $\mu = -0.732$ shows better agreement, than the simple Gaussian initial condition, albeit the former has a slight curvature.

The mean field of the stream function is shown in figure 4.5. The top half is after simulation, and the lower half corresponds to the initial state, in higher resolution though. The simple Gaussian initial condition is dramatically different from what it later developes to, yet after the simulations the two initial conditions seem to result in similar equilibria as expected. The preset slope initial mean field is largely retained.
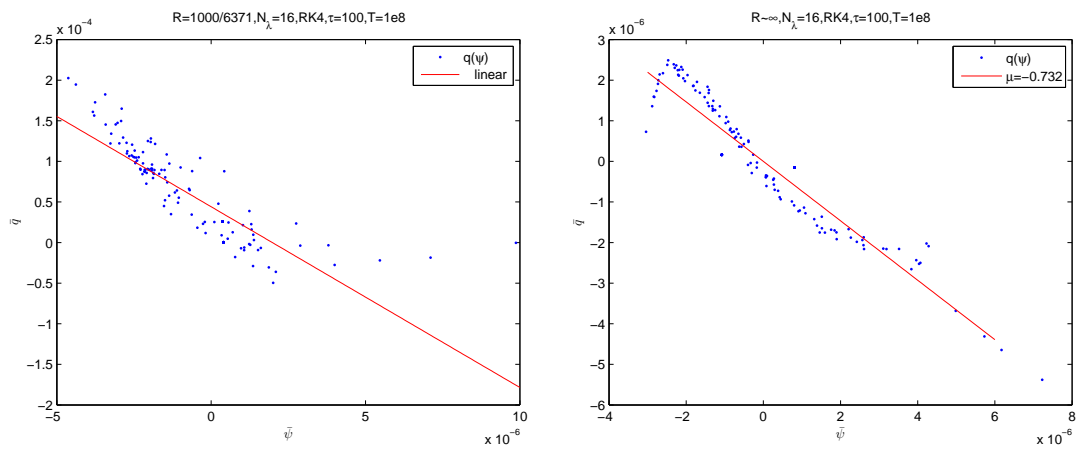
Figure 4.4: Left: Basic Gaussian $\{Q_k\}$, $R = 1000/6371$, with linear fit. Right: Preset slope $\mu = -0.732$ followed by Gaussian 'synthesis', $R = \infty$.
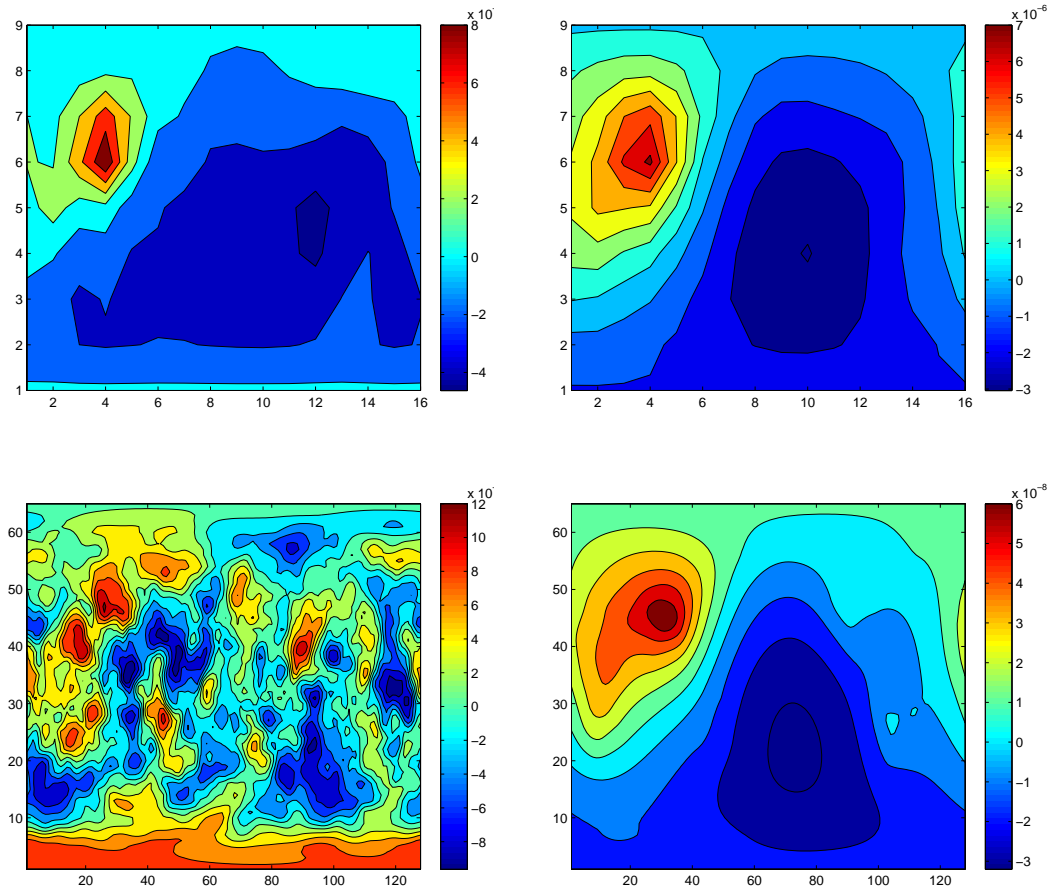
Figure 4.5: Mean field contour plots of $\bar{\psi}$. Top left: Basic Gaussian $\{Q_k\}$. Top right: Preset slope $\mu = -0.732$ with Gaussian synthesis. Bottom left: Initialized Gaussian mean field without a preset slope, $N_\lambda = 128$. Bottom right: Initialized mean field with $\mu = -0.732$ and $N_\lambda = 128$.

# Chapter 5

# Conclusions

We have seen that the implementation described in this thesis succeeds in conserving an approximation of the energy with relatively small, i.e. order $10^{-3}$ oscillations. By construction, the HPM conserves the energy up to the discretization. A finer spatial resolution increases the accuracy of the energy computation, though the same can not be said for a finer temporal resolution.

A large portion of this work was spent on understanding the peculiarities of the spherical geometry and how to handle the instabilities induced by the Eulerian grid spherical coordinate grid. In terms of modeling, this in particular includes the polar modification of the basis functions. In terms of computations, the spectral method and Spherepack are a chapter on its own.

Future work might include working with only a Cartesian coordinate system, with the spherical surface embedded in $\mathbb{R}^3$. This could even further reduce the pole problem, as has been done with the shallow water equations in [32]. This would require reformulation of the basis functions, or extension to 3D, following the approach of Ruuth [23]. Another option would be an icosahedral mesh as proposed in [24].

The large complexity of this implementation is surely worth improving. Computational advancements from Spherepack's spectral method have been widely studied by it's developers, see [28, 31].

Computing the discrete energy needs to be adjusted as described in Section 3.2 in order to thouroughly validate the method. Statistical theory should be developed for this geometry and the discretization, as it differs from the planar case. Possibly it will turn out to explain the curvature in the locus graphs 4.4. Given a full statistical theory, the many other conserved quantities only mentioned in this thesis could be numerically verified.

# Bibliography

[1] J. C. Adams and P. N. Swarztrauber. SPHEREPACK 3.0: A Model Development Facility. *Monthly Weather Review*, 127:1872–+, 1999.

[2] J. Banks, J. Brooks, G. Cairns, G. Davis, and P. Stacey. On Devaney's definition of chaos. *Am. Math. Monthly*, 99:332–334, April 1992.

[3] F. Bouchet and A. Venaille. Statistical mechanics of two-dimensional and geophysical flows. *(preprint)*, 2011.

[4] O. Bühler. Statistical mechanics of strong and weak point vortices in a cylinder. *Phys. of Fluids*, 14(7):2139–2149, 2002.

[5] G. F. Carnevale and J. S. Frederiksen. Nonlinear stability and statistical mechanics of flow over topography. *Journal of Fluid Mechanics*, 175:157–181, 1987.

[6] J. G. Charney, R. Fjortoft, and J. Von Neumann. Numerical integration of the barotropic vorticity equation. *Tellus*, 2(4):237–254, 1950.

[7] S. Dubinkina and J. Frank. Statistical mechanics of Arakawa's discretizations. *J. Comput. Phys.*, 227:1286–1305, December 2007.

[8] S. Dubinkina and J. Frank. Statistical relevance of vorticity conservation in the hamiltonian particle-mesh method. *Journal of Computational Physics*, 229(7):2634 – 2648, 2010.

[9] H. W. Ellsaesser. Expansion of hemispheric meteorological data in antisymmetric surface spherical harmonic (laplace) series. *J. Appl. Meteor.*, 5:263276, 1966.

[10] J. Frank and S. Reich. The hamiltonian particle-mesh method for the spherical shallow water equations. *Atmospheric Science Letters*, 5(5):89–95, 2004.

[11] J. E. Frank, G. A. Gottwald, and S. Reich. A Hamiltonian Particle-Mesh Method For The Rotating Shallow Water Equations. In M. Griebel and M. A. Schweitzer, editors, *Meshfree Methods for Partial*

*Differential Equations*, volume 26 of *Lecture Notes in Computational Science and Engineering*, pages 131 – 142. Springer, 2003.

[12] R. H. Kraichnan. Statistical dynamics of two-dimensional flow. *Journal of Fluid Mechanics*, 67(01):155–175, 1975.

[13] B. Leimkuhler and S. Reich. *Simulating Hamiltonian dynamics*. Cambridge monographs on applied and computational mathematics. Cambridge University Press, 2004.

[14] A. Majda and X. Wang. *Non-linear dynamics and statistical theories for basic geophysical flows*. Cambridge University Press, 2006.

[15] M. Mawson. *The shallow-water semi-geostrophic equations on the sphere*. PhD thesis, University of Reading, 1994.

[16] J. Miller. Statistical mechanics of euler equations in two dimensions. *Phys. Rev. Lett.*, 65:2137–2140, Oct 1990.

[17] P.K. Newton and T. Sakajo. The N-vortex problem on a rotating sphere: IV. Ring configurations coupled to a background field. *Proc. R. Soc. A*, 463(2080):961–977, 2007.

[18] National Institute of Standards and Technology. Digital library of mathematical functions, August 2011.

[19] J. Pedlosky. *Geophysical fluid dynamics*. Springer study edition. Springer-Verlag, 1987.

[20] L.F. Richardson. *Weather prediction by numerical process*. University Press, 1922.

[21] R. Robert. A maximum-entropy principle for two-dimensional perfect fluid dynamics. *Journal of Statistical Physics*, 65:531–553, 1991. 10.1007/BF01053743.

[22] R. Robert and J. Sommeria. Statistical equilibrium states for two-dimensional flows. *Journal of Fluid Mechanics*, 229:291–310, 1991.

[23] S. J. Ruuth and B. Merriman. A simple embedding method for solving partial differential equations on surfaces. *J. Comput. Phys.*, 227:1943–1961, January 2008.

[24] R. Sadourny, A. Arakawa, and Y. Mintz. Integration of the Nondivergent Barotropic Vorticity Equation with an Icosahedral-Hexagonal Grid for the sphere. *Monthly Weather Review*, 96:351–356, 1968.

[25] R. Salmon. *Lectures on geophysical fluid dynamics*. Oxford University Press, 1998.

[26] R. Salmon, G. Holloway, and M. C. Hendershott. The equilibrium statistical mechanics of simple quasi-geostrophic models. *Journal of Fluid Mechanics*, 75(04):691–703, 1976.

[27] W. Schubert, R. Taft, and L. Silvers. Shallow water quasi-geostrophic theory on the sphere. *Journal of Advances in Modeling Earth Systems*, 1(2), 2009.

[28] W. F. Spotz, M. A. Taylor, and P. N. Swarztrauber. Fast shallow-water equation solvers in latitude-longitude coordinates. *J. Comput. Phys.*, 145:432–444, September 1998.

[29] P. N. Swarztrauber. On the Spectral Approximation of Discrete Scalar and Vector Functions on the Sphere. *SIAM Journal on Numerical Analysis*, 16(6):934–949, 1979.

[30] P. N. Swarztrauber. The approximation of vector functions and their derivatives on the sphere. *SIAM Journal on Numerical Analysis*, 18:191–210, 1981.

[31] P. N. Swarztrauber and W. F. Spotz. Spherical harmonic projectors. *Mathematics of Computation*, 73:753–760, 2004.

[32] P. N. Swarztrauber, D. L. Williamson, and J. B. Drake. The Cartesian method for solving partial differential equations in spherical geometry. *Dynamics of Atmospheres and Oceans*, 27(1-4):679–706, January 1998.

[33] W.T.M. Verkley. A balanced approximation of the one-layer shallow-water equations on a sphere. *J. Atmos. Sci.*, 66(6), 2009.

[34] V. Zeitlin. Finite-mode analogs of 2d ideal hydrodynamics: Coadjoint orbits and local canonical structure. *Physica D: Nonlinear Phenomena*, 49(3):353 – 362, 1991.